STIS spectroscopy of nuclear gas disks in radio-loud, early-type galaxies

JACOB NOEL-STORR[1], STEFI BAUM[2], GIJS VERDOES KLEIJN[3]
CHRIS O'DEA[2], ROELAND VAN DER MAREL[2], TIM DE ZEEUW[4]
JACQUELINE VAN GORKOM[1], and MARCELLA CAROLLO[5]
(1) Columbia University, (2) STScI, (3) ESO Germany, (4) Leiden Observatory, (5) ETH Zurich

Abstract

We have taken long slit, medium resolution spectra of the gas disks in the nuclei of a complete sample of 21 nearby radio-loud early-type galaxies using the Space Telescope Imaging Spectrograph on board the Hubble Space Telescope. We present our sample selection, observations and data reduction along with initial interpretations of those data. We find that the nuclei are all compatible with a single kinematic class: rotating disks with high velocity dispersions of the order of a few hundred km s^{-1}. We find broad nuclear components on the scale of ~ 1000 km s^{-1} in 62

1.1 Introduction

A nearby radio galaxy can produce a radio jet up to ~ 1 Mpc, emerging from a central engine that resides in an active region of size $\sim 10^{-3}$ pc in its nucleus. The energy that powers the radio jets (along with the active nuclei, as much discussed in this volume) is typically believed to be produced by the accretion of matter onto a central supermassive black hole (Rees 1984). Central emission line gas is detected in virtually all nearby radio galaxies that harbor kiloparsec-scale radio jets, and this gas along with nuclear dust presumably provide the necessary sources of fuel. However, the relationship between quiescent and radio-loud early-type galaxies remains one of the mysteries in active galaxy research.

Nearby early-type galaxies with radio jets provide an opportunity to gain an understanding of the conditions that lead to the formation of an active nucleus, and of the physics of the region surrounding the black hole, where the radio jet is formed. To this end, we are undertaking a coordinated, multiwavelength study of a complete sample of the nearest radio galaxies.

Our galaxy sample (the UGC FR-I sample) contains all nearby ($v_{\rm r} < 7000$ km s^{-1}), elliptical or S0 galaxies in the declination range $-5° < \delta < 70°$ in the UGC catalog (limits magnitude $m_B < 14.6$ and angular size $\theta_p > 1.0'$) that are extended radio-loud sources (larger than $10''$ at 3σ on VLA A-Array maps and brighter than 150 mJy from single dish flux density measurements at 1400 MHz). The source information is shown in Table 1.1, including nuclear dust morphologies from Verdoes Kleijn et al. (1999) and recession velocities (v_{sys}). For further discussion of the sample see Verdoes Kleijn et al. (1999), Xu et al. (2000) and Noel-Storr et al. (2003).

We have obtained HST Space Telescope Imaging Spectrograph (STIS) medium

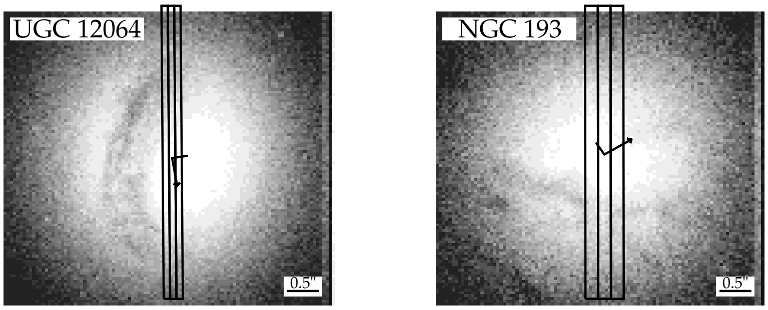

Fig. 1.1. Two STIS aquisition images illustrating typical slit arrangements (overlaid) and nuclear dust morphologies. North-east indicators are shown.

Table 1.1. *The UGC FR-I Galaxy Sample.*

Galaxy	v_{sys} (km s^{-1})	Dust	Galaxy	v_{sys} (km s^{-1})	Dust
NGC 193	4343	Lane	NGC 4261	2213	Disk
NGC 315	5093	Disk	NGC 4335	4673	Disk
NGC 383	4890	Disk	NGC 4374	1155	Lane
NGC 541	5498	Disk	NGC 4486	1155	Irreg.
NGC 741	5265	...	NGC 5127	4830	Lane
UGC 1841	6360	Disk	NGC 5141	5303	Lane
NGC 2329	5725	Disk	NGC 5490	5790	Lane
NGC 2892	6810	...	NGC 7052	4155	Disk
NGC 3801	3255	Irreg.	UGC 12064	5123	Disk
NGC 3862	6330	Disk	NGC 7626	3495	Lane
UGC 7115	6788	Disk			

resolution long slit spectra of the nuclear regions of our sample galaxies (Figure 1.1). In HST program GO-8236 we used the `G750M` grating and the `52x0.1` and `52x0.2` apertures as descibed by Kimble et al. (1998). We include data for NGC 4374 (M84) from program GO-7124 (see Bower et al. 1998) and for NGC 4486 (M87) from program GO-8666. These data are presented in full by Noel-Storr et al. (2003) and we summarize our findings here.

1.2 Analysis and Results

We performed data reduction using the standard STIS calibration pipeline (`calstis`, see Brown et al. 2002) and tools present in NOAO/IRAF and the contributed STSDAS packages.

We used a χ^2 minimization routine using Levenberg-Marquardt iterations (see

Table 1.2. *Mean kinematic parameters.*

Class	N_{Gal}	$\sigma_{\rm nuc.}$ (km s^{-1})	$\overline{\sigma_{\rm 100pc}}$ (km s^{-1})	$\Delta_{\rm 100pc}$ (km s^{-1})
Rotators	13	463 ± 254	236 ± 72	390 ± 250
Non-Rotators	7	381 ± 147	242 ± 95	149 ± 095

Press et al. 1992) to fit a template of five Gaussians (representing the Hα, [NII]$_{6550}$, [NII]$_{6585}$, [SII]$_{6718}$ and [SII]$_{6733}$ lines) to the observed spectra. The application of this fitting technique and development of this routine are described by van der Marel & van den Bosch (1998). Formal errors are drawn from the covariance matrix of the fit. As we do not expect the noise in each spectrum to be normally-distributed after the steps of wavelength calibration and two-dimensional rectification, these error values should be treated strictly as the formal fit errors under the understanding that the size of the real errors may be somewhat larger.

1.2.1 Rotating Gas Disks

By inspecting maps of the central kinematics and the velocity profiles along each slit, we have classified, by eye, the galaxies into two classes: rotators and non-rotators. Rotators are systems where we see patterns reminiscent of rotation curves; in non-rotators we find no such patterns - the kinematics seem either irregular or organized in some manner that does not represent regular rotation. We do not include NGC 741 in discussions of kinematics as the signal to noise was particularly poor. We classify 67% (N = 13/20) of the UGC FR-I galaxies as rotators, 73% of galaxies with dust disks (N = 8/11), 100% of galaxies with dust lanes (N = 5/5) and 67% of galaxies with complex dust or no dust (N = 2/3) are rotators.

We have made use of the central velocity dispersion ($\sigma_{\rm nuc.}$), the mean velocity dispersion ($\overline{\sigma_{\rm 100pc}}$) and the difference in mean velocities on each side of the nucleus ($\Delta_{\rm 100pc}$), both within $100h_{70}$ pc of the brightest pixel, as illustrative of the global kinematic parameters along the central slit. The mean parameters for each class are summarized in Table 1.2.

We find no significant systematic differences between the typical values of $\overline{\sigma_{\rm 100pc}}$ between the two classes. Using the Kolmogorov-Smirnov Test to assess the two groups we find a probability of 0.93 that the distributions of velocity dispersions were drawn from the same underlying distribution. Naturally, applying the same test to the $\Delta_{\rm 100pc}$ parameter results in the much lower probability of 0.08 that these were drawn from the same distribution.

On further investigation, we conclude that rotators and non-rotators represent the same type of kinematic systems, with observational effects such as inclination and dust properties limiting our ability to detect the rotation of those systems where we do not. We suggest that a model of a rotating gas disk with significant random motions is compatible with all of the observations.

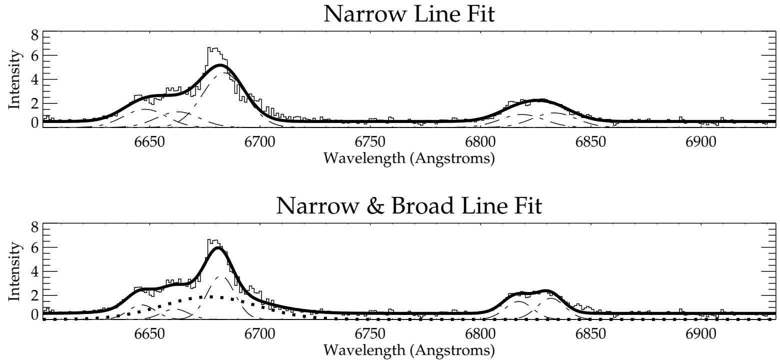

Fig. 1.2. Fits to the nuclear spectrum of NGC 193 with just narrow lines (top) and an additional broad component (bottom). A clear improvement in the fit can be seen when the broad component is included.

Table 1.3. *Comparison of broad line statistics (all units km s^{-1})*

Parameter	UGC FR-I sample (This work)	Sy/LINERs (Ho+ 1997)	Radio Loud (Sulentic+ 2000)
$\langle \sigma_{BL} \rangle$	1295 ± 218	2400 ± 1100	5900 ± 3700
$\langle \sigma_{NL} \rangle$	371 ± 153	...	...
$\langle v_{NL} - v_{BL} \rangle$	-435 ± 335	...	-500 ± 1200

1.2.2 Broad Lines?

In many cases, very close to the nucleus the fit does a poorer job of matching the observed spectra. In an attempt to improve the fit to the narrow centers of the lines we tested a fit for the central spectrum of each galaxy including an additional fit component with independent velocity, velocity dispersion and flux.

The fit to the central spectrum is improved in 62% of the galaxies by the inclusion of this component (Figure 1.2). Each of these fits resulted in the supplementary component being centered redwards of the Hα line with a velocity dispersion between about two and ten times that of the narrow lines; thus we describe this feature as a broad fit component. The detection is not dependent on dust morphology or inclination, but is a function of flux, suggesting that detection is signal to noise dependent.

The broad components could originate either as an artifact of attempting to fit Gaussians to non-Gaussian line profiles, or from a physical source – such as a broad line region or a change in the characteristics of the gas.

We detect broad components only in the central few pixels, this could be a consequence of the fall in signal to noise or that the component is an unresolved source. It is important to note as a consequence of this, that fitting single Gaussians to each line samples a different part of the line shape as the central pixels are approached.

In Table 1.3 we show the mean properties of the broad components (velocity dispersions of the broad $\langle\sigma_{BL}\rangle$ and narrow $\langle\sigma_{NL}\rangle$ lines and the velocity offset of the broad line from the Hα narrow line $\langle v_{NL} - v_{BL}\rangle$) and compare them to the samples of LINERS by Ho et al. (1997) and Radio Galaxies summarized by Sulentic et al. (2000). These comparisons show that our broad components are compatible with the broad lines seen in LINERs and that the observed offsets from the narrow line components are compatible with those observed in samples of radio loud galaxies.

1.3 Conclusions

We find that the gas in all of the nuclei in our sample is compatible with a single kinematic description: a rotating gas disk, where random motions are always important. We find that the inclusion of an additional fit component with unconstrained parameters improves our fit to the nuclear spectrum in 62% of the galaxies, where it fits in every case as a broad component in the vicinity of Hα and [NII]. The detection of the broad component is related to the line flux (and therefore the signal to noise). The broad components have a mean velocity dispersion of 1349 ± 345 km s^{-1} and are redshifted from the narrow line components (assuming an origin in Hα) by 486 ± 443 km s^{-1}.

The broad component could be a consequence of non-Gaussian line profiles with broad wings, which would be biased toward the brightest [NII] line (redwards of Hα). However, our more detailed analysis of line shape shows that it is very hard to reproduce this effect by including broad (even asymmetric) wings on each line, suggesting the broad component may indeed have a physical origin.

As we continue with this research we will model the galaxies with thin disk and spherical gas distributions (e.g. Verdoes Kleijn et al. 2002) in order to obtain estimates of the black hole masses for each galaxy. We will also extend our investigation into the ionization profiles of each nucleus; investigating the ionization properties of each nucleus and seeking the signs of jet / disk interactions.

References

Bower, G. A., et al. 1998, ApJL, 492, 111

Brown, T. et al. 2002, STIS Data Handbook, version 4.0, ed. B. Mobasher, Baltimore, STScI

Ho, L. C., Filippenko, A. V., Sargent, W. L. W., & Peng, C. Y. 1997, ApJS, 112, 391

Kimble, R., et al. 1998, ApJ, 539, 13

Noel-Storr, J., et al. 2003, ApJS, submitted

Press, W. H., Teukolsky, S. A., Vetterling, W. T., Flannery, B. P. 1992, Numerical Recipies in Fortran, 2nd Edition (Cambridge: Cambridge University Press)

Rees, M. 1984, ARA&A, 22, 471

Sulentic, J. W., Marziani, P., & Dultzin-Hacyan, D. 2000, ARA&A, 38, 521

van der Marel, R. P., & van den Bosch, F. C. 1998, AJ, 116, 2220

Verdoes Kleijn, G. A., Baum, S. A., de Zeeuw, P. T., & O'Dea, C. P. 1999, AJ, 118, 2592

Verdoes Kleijn, G. A., van der Marel, R. P., de Zeeuw, P. T., Noel-Storr, J., & Baum, S. A. 2002, AJ, 124, 2524

Xu, C., Baum, S. A., O'Dea, C. P., Wrobel, J. M., & Condon, J. J. 2000, AJ, 120, 2950